Materials Today Bio 24 (2024) 100915

Contents lists available at ScienceDirect

Materials Today Bio

journal homepage: www.journals.elsevier.com/materials-today-bio

A novel electrospun polylactic acid silkworm fibroin mesh for abdominal wall hernia repair

Xingjie Wang [a,1], Changjun Liu [b,1], Xuqi Li [a,1], Tianli Shen [a], Jie Lian [c], Jing Shi [d], Zhengdong Jiang [a], Guanglin Qiu [a], Yuanbo Wang [e], Er Meng [b,**], Guangbing Wei [a,*]

[a] Department of General Surgery, The First Affiliated Hospital of Xi'an Jiaotong University, Xi'an, 710061, Shaanxi, China
[b] School of Life and Health Sciences, Hunan University of Science and Technology, Xiangtan, 411201, Hunan, China
[c] Department of Pathology, The First Affiliated Hospital of Xi'an Jiaotong University, Xi'an, 710061, Shaanxi, China
[d] Department of Respiratory and Endocrinology, The Second Affiliated Hospital of Xi'an Jiaotong University, Xi'an, 710004, Shaanxi, China
[e] Department of Nuclear Medicine, The First Affiliated Hospital of Xi'an Jiaotong University, Xi'an, 710061, Shaanxi, China

ARTICLE INFO

Keywords:
Hernia repair
PLA-SF mesh
Biocompatibility
Adhesion
TGF-β1/smad pathway

ABSTRACT

Objective: Abdominal wall hernias are common abdominal diseases, and effective hernia repair is challenging. In clinical practice, synthetic meshes are widely applied for repairing abdominal wall hernias. However, postoperative complications, such as inflammation and adhesion, are prevalent. Although biological meshes can solve this problem to a certain extent, they face the problems of heterogeneity, rapid degradation rate, ordinary mechanical properties, and high-cost. Here, a novel electrospinning mesh composed of polylactic acid and silk fibroin (PLA-SF) for repairing abdominal wall hernias was manufactured with good physical properties, biocompatibility and low production cost.

Materials and methods: FTIR and EDS were used to demonstrate that the PLA-SF mesh was successfully synthesized. The physicochemical properties of PLA-SF were detected by swelling experiments and *in vitro* degradation experiments. The water contact angle reflected the hydrophilicity, and the stress–strain curve reflected the mechanical properties. A rat abdominal wall hernia model was established to observe degradation, adhesion, and inflammation *in vivo*. *In vitro* cell mesh culture experiments were used to detect cytocompatibility and search for affected biochemical pathways.

Results: The PLA-SF mesh was successfully synthesized and did not swell or degrade over time *in vitro*. It had a high hydrophilicity and strength. The PLA-SF mesh significantly reduced abdominal inflammation and inhibited adhesion formation in rat models. The *in vitro* degradation rate of the PLA-SF mesh was slower than that of tissue remodeling. Coculture experiments suggested that the PLA-SF mesh reduced the expression of inflammatory factors secreted by fibroblasts and promoted fibroblast proliferation through the TGF-β1/Smad pathway.

Conclusion: The PLA-SF mesh had excellent physicochemical properties and biocompatibility, promoted hernia repair of the rat abdominal wall, and reduced postoperative inflammation and adhesion. It is a promising mesh and has potential for clinical application.

A. Schematic illustration of the fabrication of PLA-SF mesh for the rat abdominal hernia model. B. A square defect was made in the abdominal ventral hernia model and repaired with PP mesh, PLA mesh and PLA-SF mesh. C. Differentiation of fibroblasts to myofibroblasts via the TGF-β/Samd pathway.

1. Introduction

A hernia occurs when an internal organ or other part of the body protrudes through the wall of muscle or tissue that it is normally contained within [1]. Hernias can be caused by, for example, congenital factors, trauma, surgery, and obesity [2]. The most common forms of hernias are inguinal hernias and abdominal hernias, of which the

* Corresponding author.
** Corresponding author.
E-mail addresses: menger@hnust.edu.cn (E. Meng), weiguangbing1208@163.com (G. Wei).
[1] These authors contributed equally to this work.

https://doi.org/10.1016/j.mtbio.2023.100915
Received 17 July 2023; Received in revised form 5 December 2023; Accepted 12 December 2023
Available online 15 December 2023

majority are incisional hernias. One billion people today will suffer from hernias during their lifetime. In some research, the incidence of incisional hernias was as high as 4–10 %[3,4] which brought a heavy burden to society.

In clinical practice, surgeons often use meshes to repair incisional abdominal wall hernias. Commonly used meshes are made of synthetic materials, such as polypropylene (PP), polytetrafluoroethylene (PTFE), and polyester (PE) [5–7]. At present, PP, a non-absorbable synthetic polymer, is the most widely used braided material for the fabrication of commercially available surgical mesh [8]. Despite its advantages, such as being chemically inert, having excellent physical and mechanical stability, and being low cost, PP mesh is not considered an ideal material as surgical mesh due to its hydrophobicity and initiation of a foreign body reaction [9]. During hernia repair, surgical meshes should be used to reinforce and replace tissues for long-term support of the abdominal wall. However, during the entire period of prosthesis implantation, postoperative complications, such as inflammation and infection [10], chronic pain [11], fibrosis and adhesions [12], and enterocutaneous fistulas [13], have been reported as a result of synthetic meshes, which has limited their wide clinical application. Postoperative adhesion is a common complication in abdominal wall hernia surgery. Despite the combination or coating with other materials, such as omega 3, poliglecaprone 25, titanium, fatty acids, sirolimus, silk fibroin, titanium, Monocryl, polyvinylidene fluoride (PVDF), and hyaluronate, which have been used to eliminate protein adsorption, there are other drawbacks that still concern surgeons [14–16].

In recent years, the use of biomaterials, such as acellular dermal matrix [17], porcine small intestinal submucosa (SIS) [18,19], silkworm silk [20], spider silk [21], collagen and elastin [22], has shown promise in hernia repair. Small intestinal submucosa (SIS) is the most commonly used biological mesh clinically, and has excellent biocompatibility and can promote tissue remodeling [23]. However, its heterogeneity, rapid degradation rate, ordinary mechanical properties, and high cost affect its wide application [24,25]. Many biological meshes are difficult to obtain and put into clinical use due to their complicated manufacturing processes and high costs compared to traditional meshes. The price of biologic mesh was over 200 times that of synthetic mesh for hospital outcomes [26]. Silkworm silk is easily available in large quantities and cheaper than SIS, and it can be seen everywhere in our lives. Furthermore, it has unique material properties, such as desirable biocompatibility, low biodegradability, and good processability [20]. Due to the maturity of electrospinning technology, the production of large-scale PLA-SF mesh has become possible. The excellent mechanical properties of silkworm silk, including exceptional strength and toughness, provide unlimited potential for the fabrication, functionalization, and processing of robust biomaterials for various clinical applications [27]. In addition, in the absence of hydrophilic sericin proteins, silk fibroin (SF) fibers are normally stronger and stiffer than undegraded silkworm silk fibers and are widely used in biomaterial research [27,28]. Furthermore, the *in vitro* and *in vivo* safety and excellent biocompatibility of SF have been evaluated in many studies [29–31].

Polylactic acid (PLA), a polymer approved by the U.S. Food and Drug Administration (FDA), is a potentially biodegradable material for clinical applications [32]. PLA produced by microorganisms has additional advantages over other polyesters due to its abundant market supply and low price. PLA was often used in biomedical materials combined with other meshes in research due to its cytocompatibility and degradability [33], but it has poor biomechanical properties with only 1 MPa of ultimate strength [34]. However, due to the advantages of electrospinning, PLA has been widely used to blend with other components to improve mechanical properties and fabricate structures [35]. Due to its low cost, high efficiency, straightforward process, and ease of incorporating additional components to create composite nanofibers. Electrospinning has attracted considerable interest and attention as a method for creating nonwoven membranes or mats with nano, submicron, or micron-sized polymer fibers [36]. Over the years, more than 200 polymers have been successfully electrospun for extensive biomedical applications, and the number is steadily rising [37].

Because of strong protein adsorption on hydrophilic surface, the improvement of the hydrophilicity and biocompatibility of synthetic materials without degrading performance is a vital direction for research and development of next-generation meshes. Therefore, in this study, an attempt was made to fabricate an absorbable, nanoporous, and anti-adhesion mesh by blending PLA with SF proteins. The combination of SF and PLA, at a ratio of 2:8, was electrospun to form a nanofibrous membrane mesh (PLA-SF mesh) for abdominal wall hernia repair, which combined the hydrophilicity, biocompatibility, and high performance of the silkworm silk with the excellent electrospinning ability of PLA. Here, we will comprehensively evaluate the properties of the new mesh, including physicochemical properties, biocompatibility and therapeutic effects on abdominal wall hernia repair in rat models. We hope that the novel compositional mesh will provide a basis for clinical use in the future.

2. Materials and Methods

2.1. Mesh preparation

PP mesh was obtained from Condiner Medical (China). PLA was purchased from NatureWorks (USA). The silkworm (*Bombyx mori*) cocoons were purchased from local cocoon collectors (Xiangtan, China), dried in a hot air oven, chopped into small pieces, and then boiled in hot distilled water containing 0.02 mol L^{-1} sodium carbonate (Na_2CO_3) for 20 min with constant stirring. The degummed cocoon silks were repeatedly washed with deionized water to remove the glue-like sericin and dried in a hot air oven at 60 °C for 24 h. The degummed silks were dissolved in 9.3 mol L^{-1} LiBr solution and then dialyzed extensively against distilled water using a 12 kDa cutoff dialysis membrane for 3 days. The distilled water was changed every 6 h to completely remove LiBr. After dialysis, the SF solution was centrifuged at 12,000 rpm for 10 min and lyophilized.

SF and PLA were dissolved together in hexafluoroisopropanol (HFIP) at final concentrations of 2 % and 8 % (w/v), respectively, while a separate solution of PLA in HFIP (final concentration 10 % (w/v)) was used as a control. The electrospinning solutions were stirred overnight to ensure that they were all completely dissolved and centrifuged at 12,000 rpm for 10 min to remove any insoluble material. For the fabrication of the electrospinning mesh, the electrospinning solution was placed in a 10 mL plastic syringe equipped with a 20-gauge needle, with an inner diameter of 0.61 mm. A positive voltage of 18 kV was applied by using a high voltage generator (Dongwen high voltage, Tianjin, China) at a distance of approximately 10 cm from the needle tip and a piece of aluminum foil as a fiber collector. The electrospinning solution was expelled into the high voltage electric field at a constant rate of 0.6 mL h^{-1} from the syringe via a syringe pump (LongerPump, Hebei, China). The electrospun scaffolds were dried in a fume hood for 24 h and then stripped from the aluminum foil. The thickness of the PLA-SF and PLA electrospun meshes was approximately 0.1 mm. The meshes were UV sterilized prior to use.

2.2. Scanning electron microscopy and energy dispersive spectrometer mapping

The PP mesh was observed at a magnification of 300 × with an acceleration voltage of 3 kV. The PLA and PLA-SF meshes were observed at magnifications of 300 × , 1500 × , and 5000 × with an accelerating voltage of 3 kV. Energy dispersive spectrometer mapping: A certain area on the surface of the sample was used as the detection area. By collecting characteristic X-ray photons, the plane distribution diagram of each element (especially C, O, and N) can be obtained, and each element is represented by different colors.

2.3. Fourier transform infrared spectroscopy (FTIR)

The infrared spectrum can identify the different functional groups present in the samples and verify whether the compound was synthesized successfully. Microinfrared spectroscopy (Bruker VERTEX70, USA) was used to study the chemical bonding and molecular structure of PLA and PLA-SF meshes. The transmittance of the two samples in the range of 4000 to 400 cm^{-1} was analyzed.

2.4. Water contact angle

The water contact angle test was performed to measure the hydrophilicity of both PLA and PLA-SF meshes. First, the meshes were adhered to the cover slide, which ensured that the meshes were flat. Second, 5 μL deionized water was dropped onto the meshes. Third, photos were captured by a digital microscope (U500X, Denmark). Finally, the contact angle was determined by using ImageJ software.

2.5. Stress–strain curve

The meshes were cut into long strips with a size of 1 cm × 3 cm, and 0.5 cm of each end of the longitudinal axis was fixed on the instrument to expose test pieces of the meshes with a size of 1 cm × 2 cm. A Bose Electroforce load testing device was used to test the meshes under tensile forces at a strain rate of 0.1 mm/s. The yield point, elastic modulus, ultimate strength, and maximum elongation of the meshes were obtained. The calculation range of the elastic modulus of the meshes should be the elastic deformation region of the material. The formula is λ = stress/strain.

2.6. Swelling and degradation in vitro

The three meshes were cut into 3 cm × 3 cm squares, soaked in PBS, and placed in a 37 °C incubator for 90 days. The size of the mesh was measured, and its weight was measured after drying.

2.7. Surgical procedures

All animal experiments were carried out with the approval of the Ethics Committee of the Xi'an Jiaotong University Center for Health Sciences. A total of 128 SD rats weighing 200 g ± 20 g were purchased from the SPF animal room of the Xi'an Jiaotong University Health Science Center. All rats were housed in a 12-h/12-h light/dark cycle at 25 °C and 60 % ± 10 % humidity with free access to food and water. All rats were randomly divided into four groups. The rats in the first three groups were implanted with PP, PLA, and PLA-SF meshes, while the rats in the fourth group were not implanted with any mesh. The rats were anesthetized with isoflurane (0.6–0.8 L/min), and their skin was disinfected with Aner iodine. A 4-cm abdominal incision was made, and then the subcutaneous tissue and fascia were separated by electrocautery. A square defect of 2 cm × 2 cm was made with the linea alba as the center. The PP, PLA, and PLA-SF meshes were cut into 3 cm × 3 cm squares, and the abdominal wall muscles around the defect were overlapped with 0.5 cm overhangs on each side. The four corners of the meshes were sutured to the abdominal wall muscle with 5-0 PGLA (Jinhuan®, China), and the midpoints of the four sides of the mesh were fixed if necessary. The skin was continuously sutured with 4-0 Mersilk (Ethicon, USA). In the sham group, only the abdominal wall was incised, and the hernia was not repaired. The rats were placed on a heating pad to keep warm during the operation until they woke up.

After the operation, the rats were reared in cages, with 4 rats in each cage, and mortality, recurrence rate, infection rate, incidence of seroma, change in body weight and activity were observed. Rats were sacrificed with excess chloral hydrate on days 1, 3, 5, 7, 15, 30, 60, and 90. The meshes were collected along with the muscle tissue under the mesh. The samples were divided into 3 parts: one for histology, one for RNA extraction, and one for protein extraction.

2.8. Open field test

The open field test is commonly used to assess anxiety, exploration, and exercise. It was carried out on an unfamiliar square stage, and the field (625 mm long × 740 mm wide) was divided into 25 squares and surrounded by walls approximately 510 mm high. One day after surgery, the rats were placed in the arena for 5 min, and the behavior of the rats was recorded on a computer with the OFT-100 opening event test system (Techman, China). Several categories of behaviors can be scored, such as movement and exploration. Here, we were more concerned about the movement distance of the rats after operation. The arena was wiped with 75 % alcohol and allowed to dry before each test.

2.9. Degradation in vivo

After SD rats were sacrificed, a U-shaped incision was made to observe whether the mesh was displaced, shrunken, or degraded. The degradation rate was evaluated by the remaining area of the mesh.

2.10. Evaluation of intraperitoneal adhesions

The abdominal wall was opened with a U-shaped incision. Adhesion between the mesh and intra-abdominal region was observed and scored according to the grades shown in Supplementary Table 1. Briefly, adhesions that can be easily broken are grade 1, those that can be separated with instruments are grade 2, and those that are difficult to separate or cause organ damage after separation are grade 3.

2.11. Micro-CT

After 90 days of hernia repair, the rats were anesthetized, and any development abdominal adhesions was observed following the gentle injection of 20 mL of air into the abdominal cavity. For micro-CT imaging, the rats were placed in the supine position. Micro-CT images were obtained using a SkyScan 1176 (Bruker, Belgium) with a resolution of 9 μm.

2.12. Hematoxylin and eosin staining and Masson staining

The tissues were fixed with 4 % paraformaldehyde (PFA) at room temperature for 24 h. After dehydration and paraffin embedding, the tissues were cross-sectioned to a thickness of 3–5 mm, stained with HE and Masson, and photographed by a Phmias Microscope (MC-D310U/C, China) at a magnification of 200 × . Five fields of view were taken. The results of HE staining were scored by 2 experts. The number of inflammatory cells was counted and scored according to Supplementary Table 2.

2.13. Immunofluorescence staining

Paraffin-embedded sections of tissues were deparaffinized and subjected to antigen extraction. Antibodies were diluted in PBS containing 1 % BSA and 0.01 % Triton X-100 and then added to each tissue section. The sections were placed at 4 °C overnight. A secondary antibody and DAPI were applied and examined using a fluorescence microscope (DM IL LED, Leica, Germany) at a magnification of 100 × .

The following antibodies were used for immunofluorescence analysis: CD31 (376764, Santa Cruz), PDPN (376962, Santa Cruz), α-SMA (19245, Cell Signaling Technology), Alexa Fluor 488/594 conjugated goat anti-rabbit IgG (H + L) cross-adsorbed secondary antibody (11006/11007, Thermo Fisher) and DAPI (9542, Sigma).

2.14. Cell culture

Mouse L929 fibroblasts (CL-0137, Procell, China) were cultured in DMEM (11995500, Gibco, USA) supplemented with 10 % fetal bovine serum (10091148, Gibco, USA) and 1 % penicillin–streptomycin (15140163, Gibco, USA) and incubated at 37 °C in a 5 % CO_2 humidified incubator. The medium was changed every two days. When 80 % confluence was reached, cells were digested with 0.25 % trypsin for 30 s at 37 °C and centrifuged at 800 rpm for 3 min. Cells in an exponential growth period were used in all experiments.

The three kinds of meshes were cut into 3 cm × 3 cm squares and then sterilized by UV. Cells were seeded in culture at a density of 1 × 10^6 cells/mL. After the cells adhered, the three types of meshes were placed on the plates. Cells were imaged by a microscope (DM IL LED, Leica, Germany) at 12 h, 24 h, and 48 h. Five visual fields (100 ×) were randomly selected. Cells were harvested when they were 100 % confluent.

2.15. Cell counting kit assay

L929 cells were seeded in 96-well plates (approximately 5 × 10^3 cells/well) and cocultured with three types of meshes for 12 h, 24 h, and 48 h. Then, the media was carefully removed, and the cells were cultured in 90 μL DMEM supplemented with 10 μL CCK8 reagent (C0005, TargetMol, USA) at 37 °C for 2 h. The plate was then placed on a shaker (SLK-O3000-S, Scilogex, USA) for 5 min before testing. Finally, the optical density at 450 nm (OD_{450}) was read with a microplate reader (Varioskan Flash, USA).

2.16. Transwell assay

The migration ability of L929 cells cocultivated with meshes was assessed by the Transwell assay. First, 500 μL of DMEM supplemented with 10 % FBS was added to a 24-well plate, and then the upper inserts (8 μm, Corning, USA) were placed on a 24-well plate. Next, 5 × 10^4 L929 cells were added to the upper inserts incubated with 100 μL serum-free DMEM. After 24 h of incubation, the inserts were removed from the 24-well plates and cells were fixed with 4 % paraformaldehyde for 5 min and stained with crystal violet for 30 min. Nonmigrated cells in the upper layer of the inserts were gently wiped out by cotton balls. The migrated cells were imaged by a microscope. Five visual fields (100 ×) were randomly selected.

2.17. Live/dead assay

Similar to the CCK8 assay, after coculture with three kinds of meshes for 24 h, 100 μL of Live/Dead working solution (L3224, Thermo Fisher Scientific, USA) was added to 96-well plates and the plates were incubated in dark conditions for 20 min. The cells were imaged by fluorescence microscopy (DM IL LED, Leica, Germany). Five visual fields (100 ×) were randomly selected.

2.18. Western blotting

All proteins were extracted from adhesion tissues or L929 cells with radioimmunoprecipitation assay (RIPA) lysis buffer and 5 % phenylmethanesulfonyl fluoride (PMSF). The protein samples were mixed with 5 × SDS–PAGE sample loading buffer and then boiled at 90 °C for 10 min. After sodium dodecyl sulfate–polyacrylamide gel electrophoresis (SDS–PAGE), the samples were separated, transferred to nitrocellulose membranes, blocked with 5 % skim milk for 1 h at room temperature, incubated with primary antibodies overnight at 4 °C, and then incubated with a goat or mouse anti-rabbit secondary antibody for 1 h at room temperature. The corresponding proteins were finally visualized by using electrogenerated chemiluminescence (ECL) reagents and quantified by using ImageJ software.

The primary antibodies used in this study were anti-Collagen I (ab260043, Abcam), anti-collagen III (ab184993, Abcam), anti-Bax (2772, Cell Signaling Technology), anti-Bcl-2 (ab59348, Abcam), anti-IL-1β (ab283818, Abcam), anti-TNF-α (ab205587, Abcam), anti-E-cadherin (4472, Cell Signaling Technology), anti-Vimentin (46173, Cell Signaling Technology), anti-α-SMA (19245, Cell Signaling Technology), anti-TGF-β1 (ab179695, Abcam), anti-Smad2/3 (C8685, Cell Signaling Technology), anti-P-smad2 (18338, Cell Signaling Technology), anti-P-smad3 (SC517575, Santa Cruz), and anti-Smad4 (46535, Cell Signaling Technology), and anti-GAPDH (5174, Cell Signaling Technology).

2.19. Statistical analysis

GraphPad Prism 9.0, Origin 2022, and ImageJ 2.0 were used to process the data, and the experimental data were expressed as the mean ± standard deviation (x ± SD). T-test and ANOVA were used for normally distributed data and Kruskal-Wallis H was used for non-normal data. $P < 0.05$ was considered statistically significant.

3. Results

3.1. Characterization of the three meshes

The commercial PP mesh was transparent and braided in a warp-knitted arrangement. The PLA and PLA-SF meshes were fabricated by electrospinning nanofibers and appeared white. Three types of meshes were cut into 3 cm × 3 cm squares. After the meshes were soaked in PBS buffer, the appearance of the PP and PLA meshes did not change, while the PLA-SF mesh became transparent immediately, demonstrating its high hydrophilicity. When the three meshes were dry after placing in PBS for 90 days, the PLA-SF returned to white, while the PP and PLA meshes were still unchanged. Furthermore, the three types of meshes did not swell, shrink, or degrade within 90 days (Fig. 1A). The weights of the three meshes were 25.4 ± 1.8 g/m^2, 20.1 ± 0.6 g/m^2, and 21.3 ± 0.6 g/m^2, respectively (Fig. 1B). The alignment and morphology of the fibers of the three meshes were observed by SEM. As demonstrated in Fig. 1C-D, the commercial PP mesh was braided by fibers with a diameter of approximately 1502.67 ± 6.80 μm, while PLA and PLA-SF were successfully electrospun into nonwoven membranes by continuous and smooth-surface nanofibers with diameters of approximately 1.35 ± 0.04 μm and 1.24 ± 0.04 μm, respectively. The fiber diameter of the PP mesh was more than 1000 times larger than that of the PLA and PLA-SF meshes. Compared with the PLA mesh, the fiber surface the PLA-SF mesh was clearly more heterogeneous, which indicated the successful synthesis of the chimeric mesh.

The compositional distribution of the two meshes was investigated by EDS mapping, EDS mapping shows that the N content in the PLA-SF mesh accounts for 13.7 %, and there is no N in the PLA mesh (Fig. 2A-B). The FTIR spectra of the PLA and PLA-SF meshes are shown in Fig. 2C. The regions of interest of PLA were peaks at 1780 cm^{-1} for the C═O stretch, 1180 cm^{-1} for the C–O stretch and 1080 cm^{-1} for the C–*O*–C stretch. In addition, the peak at 1627 cm^{-1} corresponds to the amide I band of the protein, and the peak at 1511 cm^{-1} corresponds to the amide II band of the protein. This indicated that the PLA-SF mesh was successfully synthesized.

As illustrated in Fig. 2D and Supplementary Table 3, although the yield point and ultimate strength were similar, the elastic modulus of the PLA mesh was approximately 3.61 times higher than that of the PP mesh, indicating that the PLA mesh had more resistance to deformation, and the breaking elongation of the PP mesh was approximately 2.9 times higher than that of the PLA mesh, probably due to the warp-knitted arrangement of the PP mesh. After blending SF into PLA, the yield point, elastic modulus, and ultimate strength of the PLA-SF mesh were increased to 5.49, 51.04, and 4.07 times that of the PP mesh and 4.82, 14.15, and 4.24 times that of the PLA mesh, respectively. Compared

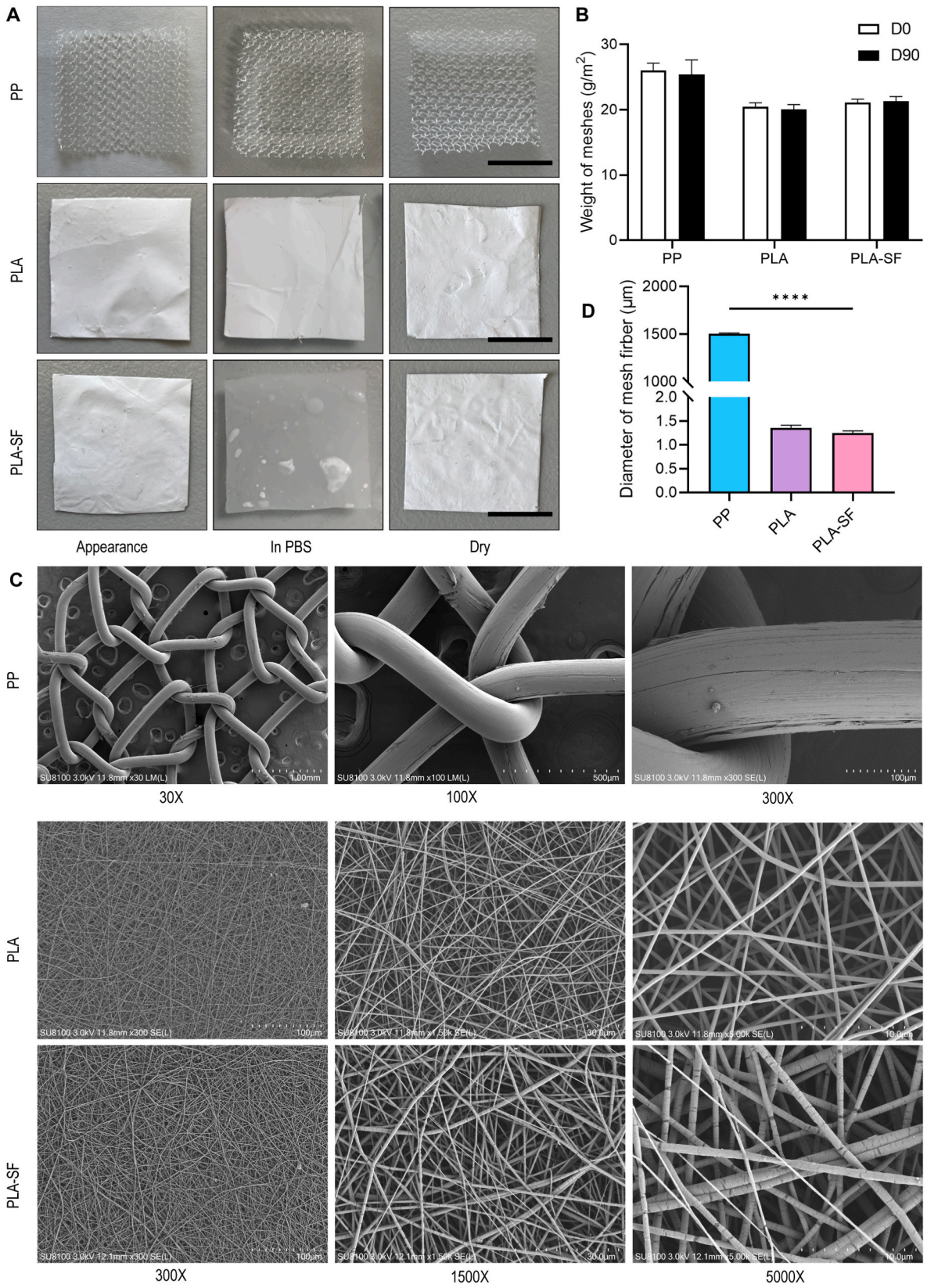

Fig. 1. Characterization of the three meshes. A) Meshes (3 cm × 3 cm) swelling and degrading in PBS. Scale bars, 1 cm. B) Weights of three meshes. C) Light microscopy and SEM image of three meshes. D) Fiber diameters of three types of meshes. ****$P < 0.0001$. *t*-test, One-way ANOVA. All experiments were performed in triplicate.

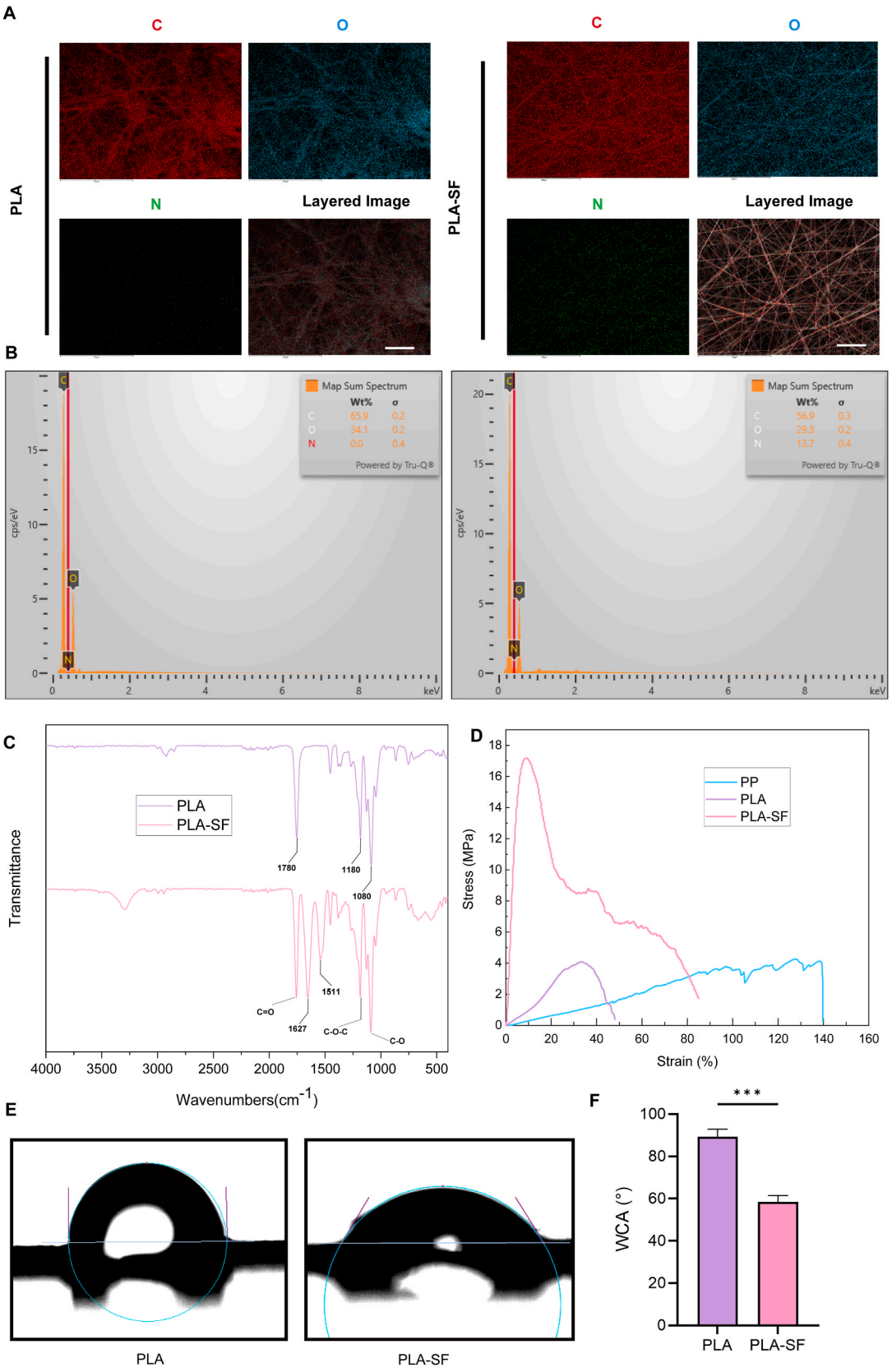

Fig. 2. Characterization of meshes. A) Representative EDS layered image of the PLA and PLA-SF meshes. B) EDS elemental mapping (the top three most abundant elements) of the PLA and PLA-SF meshes. C) FTIR of the PLA and PLA-SF meshes. D) Stress–strain curves of the PP, PLA, and PLA-SF meshes. E) Water contact angle of the PLA and PLA-SF meshes. D) Quantification of the water contact angles of the three meshes. ***$P < 0.001$. *t*-test. All experiments were performed in triplicate. Scale bar, 10 μm.

with the PLA mesh, the breaking elongation of the PLA-SF mesh was also improved 1.75 times, although lower than that of the PP mesh. It was demonstrated that the PLA-SF mesh combined the advantages of both the PP mesh and PLA mesh.

Due to the microporous structure of the PP mesh, the water contact angle of the PP mesh could not be measured. As illustrated in Fig. 2E-F, the water contact angle of the PLA mesh was significantly larger than that of the PLA-SF mesh, which demonstrated that the PLA-SF mesh exhibited better hydrophilicity.

3.2. Animal surgery

All rat abdominal wall hernia models were successfully manufactured. No rats died, no seroma or infection occurred after the operation, and there was no recurrence of hernia in any group except one case of recurrence of incisional hernia at 60 days in the PLA group. Rats were weighed for 15 days after the operation, and the difference in body weights between groups was less than 5 %, which indicates that the different meshes did not have an effect on the body weights of rats and shows that the rats maintained normal diets and no complications occurred, such as intestinal obstruction (Fig. S1).

To explore how different meshes affect the movement of the rats, an open field test was carried out. One day after the operation, the rats were placed in the field to move freely for 5 min, and the camera recorded their movement track and distance. The rats in the control group that did not receive any treatment traveled the greatest distance, while the rats in the sham group without any mesh for hernia repair moved the least, likely because they were reluctant to move due to pain. After being treated with the PP mesh, the rats moved greater distances than those in the sham group, probably due to the pain-relieving effects. Furthermore, in the PLA-SF and PLA groups, the rats had the smallest foreign body reaction and moved greater distances than the rats in the PP group (Fig. 3A and C).

3.3. Degradation and adhesion of PLA-SF mesh after tissue remodeling in vivo

None of the meshes were displaced. Half of the PP meshes shrank at

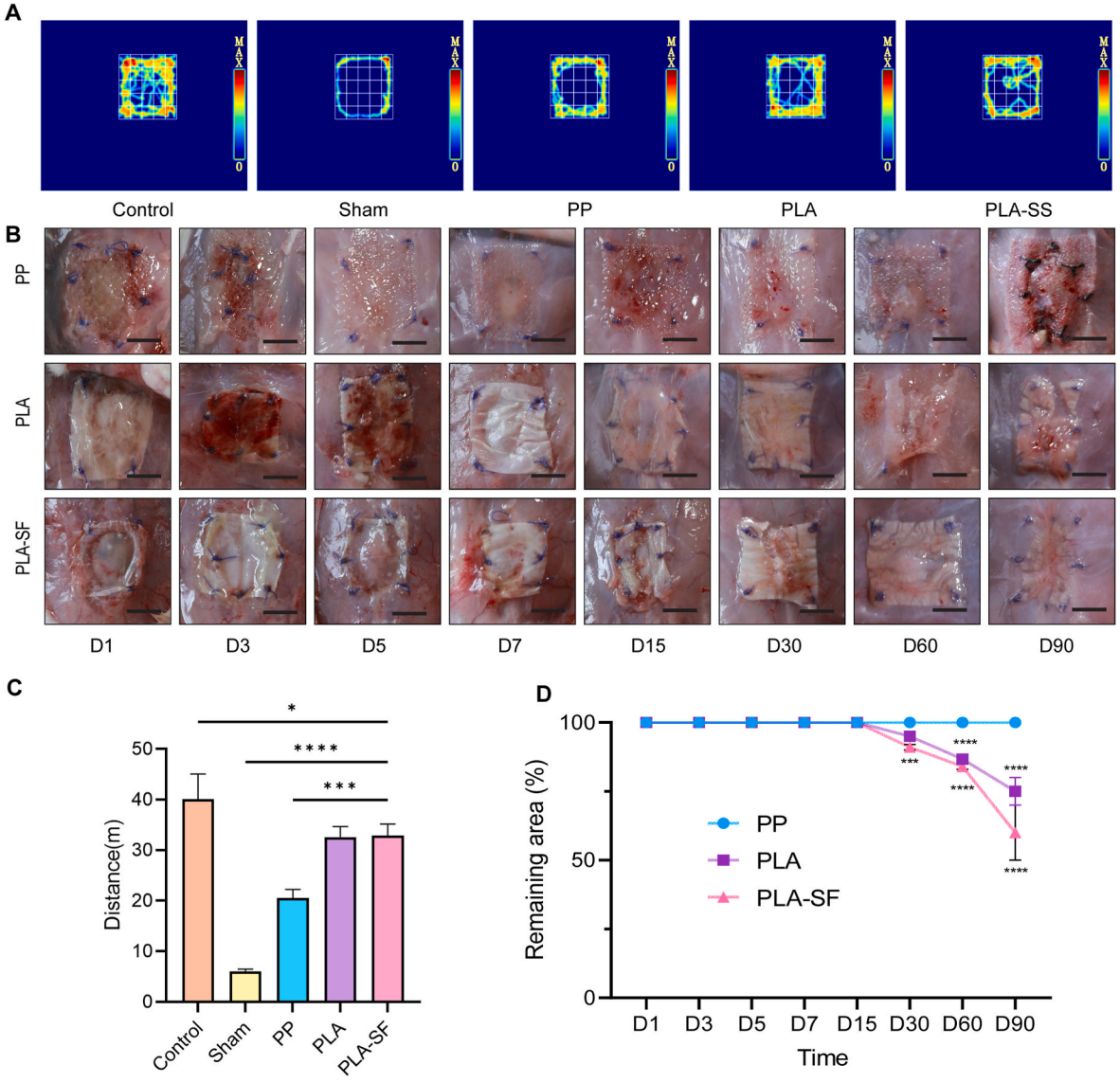

Fig. 3. General condition of the rat after surgery and *in vivo* degradation of the meshes. A) Representative heatmaps of the moving distance of rats after the operation. B) Degradation of three kinds of meshes from 1 day to 3 months after the operation. C) Quantification of the movement distance of rats treated with different meshes. D) Quantification of the remaining area of the three meshes. Scale bar, 1 cm. Data are presented as the mean ± SD ($n = 4$). *$P < 0.05$, ***$P < 0.001$. One-way ANOVA. All experiments were performed in triplicate.

90 days, possibly due to the stiff properties of the PP, while the other two meshes did not shrink over time. The PP mesh did not degrade at any time point from 1 day to 3 months. The PLA mesh began to degrade partially at 2 months, and the *in vivo* environment accelerated the degradation of the mesh compared to the *in vitro* environment. Similar to the PLA mesh, the PLA-SF mesh began to degrade at 2 months and showed 40 % degradation at 3 months, at which time the tissue remodeling had been completed (Fig. 3B and D).

In the PP group, intraperitoneal adhesion occurred on the third day, and the degree of adhesion gradually increased. On the 30th day, a dense adhesion appeared. Similar to the PP group, the degree of adhesion gradually increased with time in the PLA group, adhesion appeared on day 15, and dense adhesions appeared on day 90. Adhesions did not occur in all trials in the PLA-SF group, which might be related to the high hydrophilicity and biocompatibility of PLA-SF (Fig. 4A-B).

After 90 days of hernia repair, the rats were imaged with CT in the supine position to observe the location of the mesh and the adhesion of the abdominal cavity. Because the meshes were too thin and filled with tissues, the positions of the meshes were difficult to observe from CT images but could be observed from the location of the linea alba. The adhesion area between the PP mesh and the abdominal cavity was considerably larger than that between the PLA mesh and the abdominal cavity, while no adhesion occurred in the PLA-SF mesh group (Fig. 4C).

After 90 days of hernia repair, to evaluate the effect of meshes on intraperitoneal adhesion at the molecular level, the levels of collagen I, and collagen III in tissues were analyzed by Western blot. The expression level of collagen I in the PLA-SF group was higher than that in the PLA group and PP group, while the expression of collagen III in the PLA-SF group was lowest. An increase in type I collagen and a decrease in type III collagen results in reduced hernia formation and recurrence [38]. We speculate that the increase in type I collagen and the decrease in type III collagen are beneficial to tissue remodeling (Fig. 4D–F).

The HE staining results showed that the inflammatory response of the PLA-SF group was milder than that of the other two groups at an early stage. The inflammatory response in the PP group and the PLA group was intense during the first 7 days, and the inflammatory cell scores were up to 3 or 4 on the seventh day after surgery, while the scores of the PLA-SF group were only 1 or 2. Additionally, 15 days after surgery, the inflammation in the PLA-SF group continued to increase, but it was lower than that in the other two groups. Finally, the inflammatory response gradually decreased after 1 month (Fig. 5A and D).

CD31, a marker of vascular endothelial cells, was expressed in most cells of the PLA-SF group, suggesting more neoangiogenesis. PDPN, a marker of peritoneal mesothelial cells, was also expressed most extensively in the PLA-SF group, indicating that the peritoneum was being repaired. The increase in both CD31 and PDPN contributed to the repair

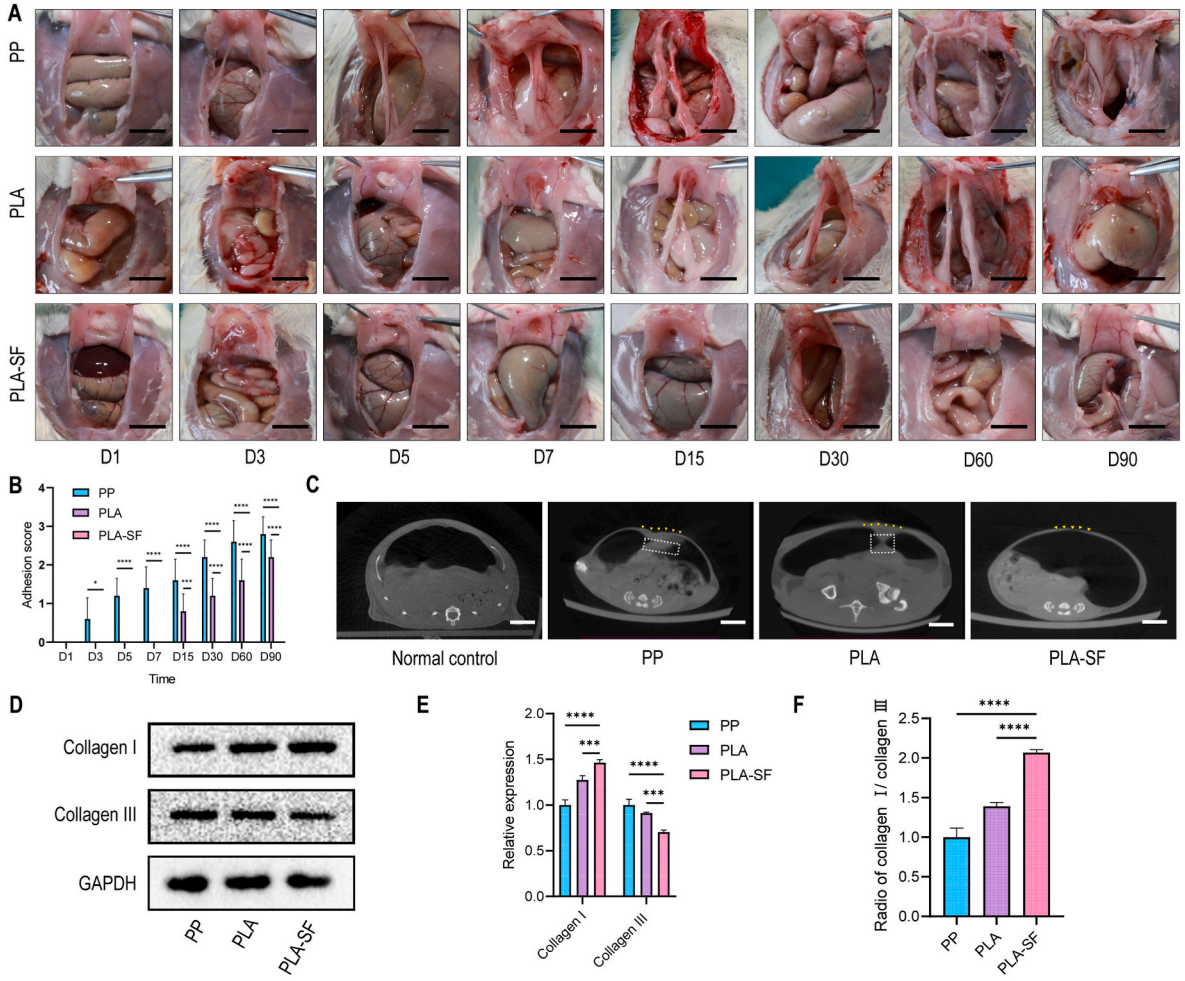

Fig. 4. The effect of the three types of meshes on adhesion formation. A) Formation of abdominal adhesion with three kinds of meshes from 1 day to 3 months after the abdominal defect was repaired. B) Quantification of adhesion. C) Representative CT images of normal control mice and mice repaired with three types of meshes 90 days after abdominal hernia repair. D) Representative Western blots of collagen expression in adhesion tissue 90 days after operation. E) Quantification of collagen expression in adhesion tissue 90 days after operation. F) The ratio of two kinds of collagen. Data are presented as the mean ± SD ($n = 4$). The triangle (yellow) represents the meshes, and the rectangle (white) represents the adhesion. Scale bar, 1 cm $^{*}P < 0.05$, $^{***}P < 0.001$, $^{****}P < 0.0001$. Kruskal-Wallis, One-way ANOVA. All experiments were performed in triplicate.

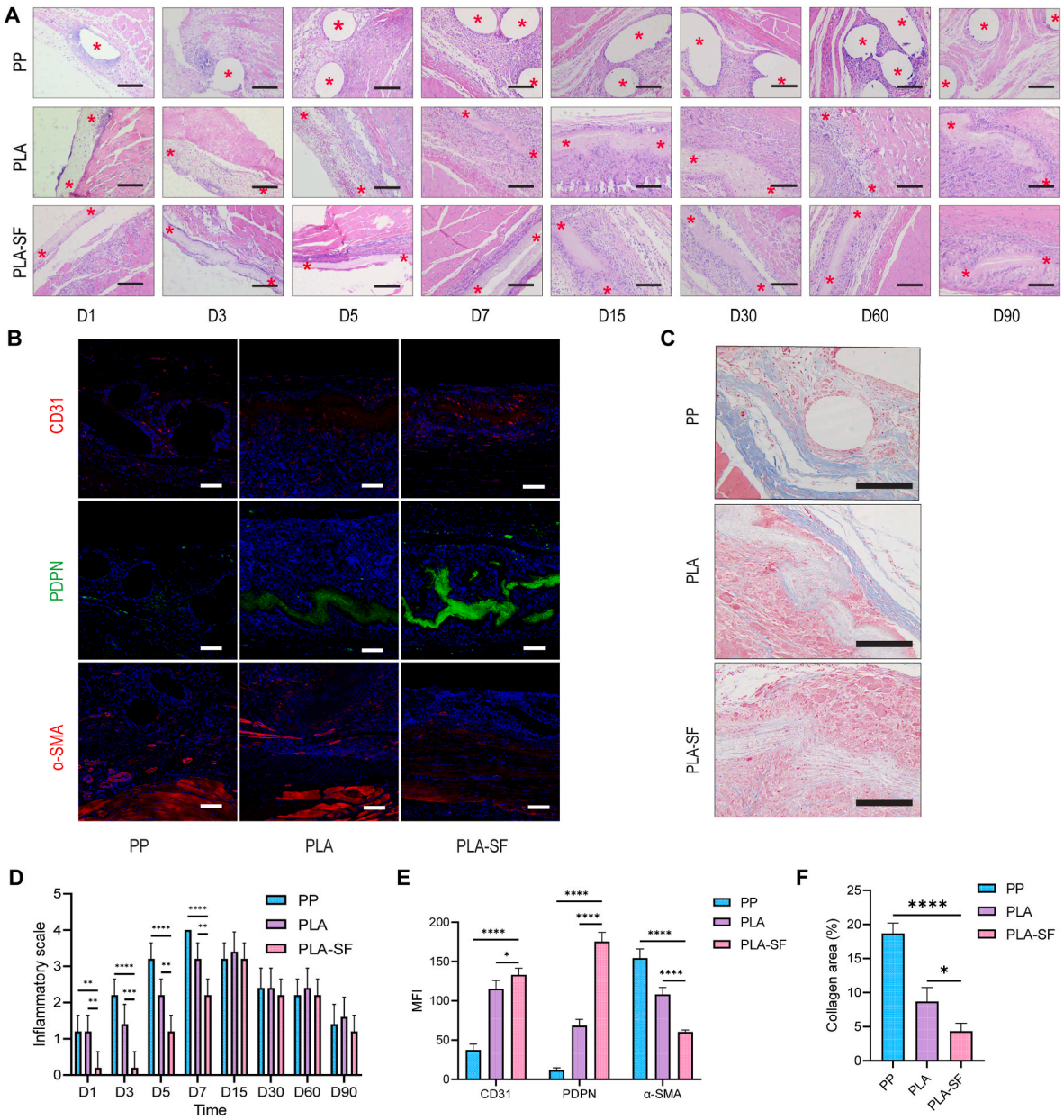

Fig. 5. Pathological changes in rats after surgery. A) Representative HE staining at different time points after surgery. B) Representative images of CD31, PDPN, and α-SMA expression in tissue 90 days after the operation. C) Representative Masson's trichrome staining 90 days after surgery. D) Quantification of inflammation. E) Mean fluorescence intensity (MFI) of CD31, PDPN, and α-SMA. F) Quantification of Masson's trichrome staining. Data are presented as the mean ± SD ($n = 4$). Scale bar, 100 μm. Red asterisks represent meshes. *$P < 0.05$, **$P < 0.01$, ****$P < 0.0001$. Kruskal-Wallis H, One-way ANOVA. All experiments were performed in triplicate.

of the abdominal wall muscles. A marker of myofibroblasts, α-SMA, was expressed the least in the PLA-SF group, which also showed the least adhesion (Fig. 5B and E). In addition, Masson trichrome staining showed less collagen deposition in the PLA-SF mesh (Fig. 5C and F).

3.4. PLA-SF promotes cell proliferation through the TGF-β1/smad pathway in vitro

To verify whether the three types of meshes could affect cell proliferation *in vitro*, L929 cells were cultured with three kinds of meshes. The results of the CCK8 assay demonstrated that there were no significant differences in cell proliferation among the four groups after 12 h. After 24 h, the cell proliferation rates of the three mesh groups were all higher than those of the control group, and the cell proliferation rate in the PLA-SF group was lower than that in the PP group, and was roughly the same as that in the PLA group (Fig. S2). The results of the Transwell assay indicated that culture with meshes after 24 h changed cell polarity and enhanced cell migration, which might be associated with adhesion formation (Fig. 6A and C). Additionally, the results of the Live/Dead assay showed that coculture with meshes after 24 h did not cause excessive cell death (Fig. 6B and D).

The three types of meshes cocultivated with L929 cells acted as foreign bodies and brought mechanical stimulation to cells, resulting in different expression of proteins. We found that L929 cells proliferated through the TGF-β1/Smad pathway. All meshes increased the expression of TGF-β1, P-Smad2/3, and Smad4 (Fig. 7A-B). The results of HE staining suggested that the three types of meshes cause cells to secrete inflammatory factors. The increased expression of IL-1β and TNF-α also confirmed this finding (Fig. 7C-D). The upregulation of the fibrotic molecules Vimentin and α-SMA and the downregulation of the cell

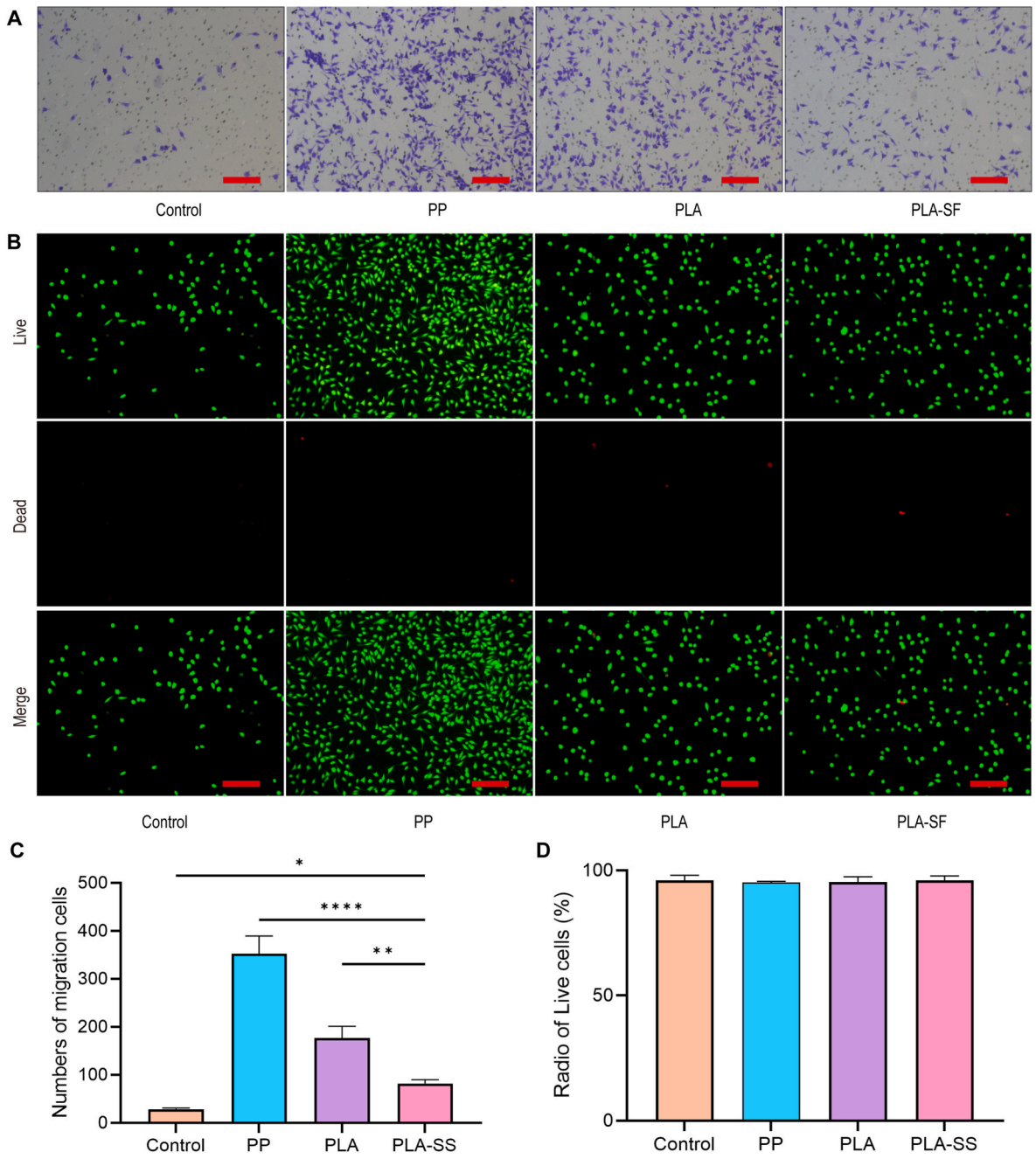

Fig. 6. Coculture with meshes promotes L929 proliferation. A) Representative images of the migration viability of L929 cells 24 h after coculture with meshes. B) Representative Live/Dead staining images showing cell viability. C) Quantification of migrated cells. D) Quantification of cell viability 24 h after coculturing with meshes. Data are presented as the mean ± SD ($n = 3$). Scale bar, 200 μm $^{*}P < 0.05$, $^{**}P < 0.01$, $^{***}P < 0.001$. One-way ANOVA. All experiments were performed in triplicate.

adhesion molecule E-cadherin indicated that both the number of myofibroblasts and the migration ability of the cells increased, which was consistent with the results of the Transwell assay (Fig. 7E-F).

4. Discussion

Surgical repair of abdominal wall hernias is one of the most common surgical procedures performed by surgeons. Before 1958, primary suture repair was used to treat abdominal wall hernias. Since the introduction of PP mesh in 1958, synthetic mesh has become the typical strategy for hernia repair. Until now, the mesh used in hernia repair surgery for many years was still PP mesh, but the various postoperative complications have driven the search for a more suitable replacement. Meshes used clinically or in research have been combined with each other or coated with PLA [2], chitosan [39], fibrin [40], amino acids [41], drugs [42], cytokines [18] or other materials to form a new type of composite mesh. However, an ideal mesh has not been found for Clinical application. An ideal mesh would have good mechanical properties and not swell and shrink, would have properties of high hydrophilicity, degradability, anti-inflammation, and anti-adhesion and would be low in price. The PLA-SF mesh in this study meets the ideal characteristics mentioned above to a certain extent.

In this study, a novel PLA-SF composite biological hernia mesh was successfully fabricated by electrospinning PLA and SF at a ratio of 8:2. Swelling experiments, degradation experiments, SEM experiments, and stress–strain tests were carried out to evaluate the physicochemical

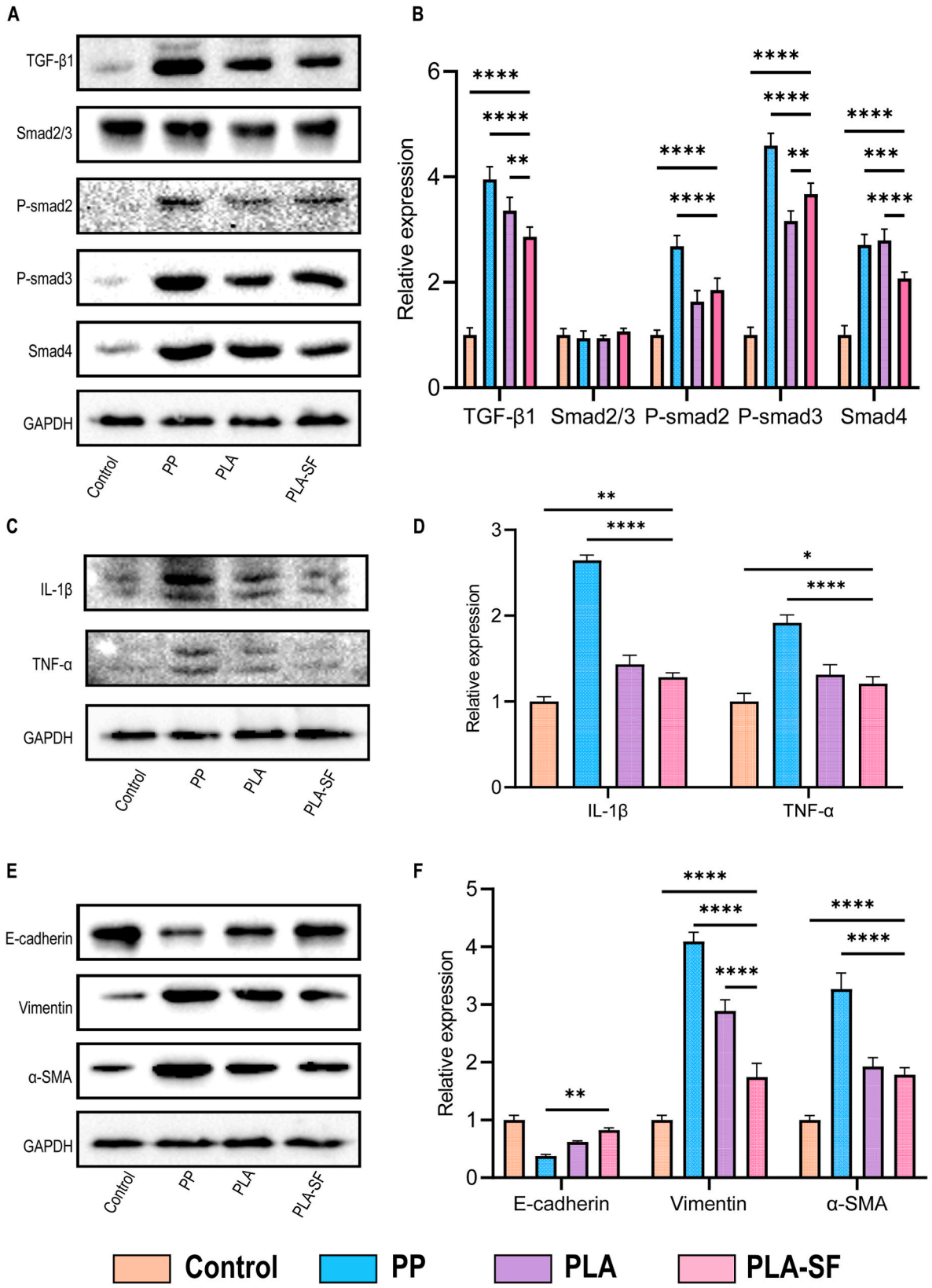

Fig. 7. The PLA-SF mesh promotes cell proliferation through the TGF-β1/Smad pathway *in vitro*. A) Representative Western blots of TGF-β1/Smad pathway-related proteins after L929 cells were cocultured with PP, PLA, and PLA-SF. B) Quantification of TGF-β1/Smad pathway-related proteins. C) Representative Western blots of inflammation-related proteins after L929 cells were cultured with PP, PLA and PLA-SF. D) Quantification of inflammation-related proteins. E) Representative Western blots of fibrotic-related proteins after L929 cells were cultured with PP, PLA, and PLA-SF. F) Quantification of fibrotic-related proteins. Data are presented as the mean ± SD ($n = 3$). $^{*}P < 0.05$, $^{**}P < 0.01$, $^{***}P < 0.001$, $^{****}P < 0.0001$. One-way ANOVA. All experiments were performed in triplicate.

properties of the new mesh. *In vivo* degradation, intraperitoneal adhesion, and inflammation were observed in a rat abdominal wall hernia model. Finally, *in vitro* coculture experiments indicated that PLA-SF mesh reduced the expression of inflammatory and fibrotic molecules and increased cell proliferation and migration, which were beneficial to tissue remodeling. Compared with the PP and PLA meshes, the novel PLA-SF mesh had excellent physicochemical properties and biocompatibility and could be a very promising composite biological mesh for hernia repair.

The abdominal wall bears the highest stress when people cough or jump (14.35 kPa and 22.80 kPa, respectively) [43]. In this study, the PP, PLA, and PLA-SF meshes could withstand ultimate strengths of 4.25 ± 0.31 MPa, 4.08 ± 0.44 MPa, and 17.28 ± 1.65 MPa, respectively, which were much higher than the stresses that the abdominal wall muscles could support, and the PLA-SF mesh performed best. Tension-free herniorrhaphy was used in hernia repair. If the mesh shrank or swelled, it changed the tension around the defect. Mesh shrinkage led to increased tension around the defect, and mesh expansion led to the protrusion of the abdominal contents, both of which could increase the recurrence rates of hernia. The PLA-SF mesh did not shrink or expand with time, and no recurrent hernias were observed.

The physical structure of the mesh affected the repair of the hernia. A study by Qiu et al. [44] showed that lightweight mesh had a less inflammatory response due to its softness, strong elasticity, and large pore size and had better histocompatibility than heavyweight mesh. Although the weight of the PP mesh used in this study was 25.4 ± 1.8 g/m^2, which is thus classified as a lightweight mesh, it still caused serious adhesions. The PLA-SF mesh weighed 21.3 ± 0.6 g/m^2 and is thus also classified as a lightweight mesh. Although it did not meet the characteristics of a large pore size, its high porosity observed with SEM promoted tissue ingrowth, caused a reduced foreign body reaction and lower inflammation, and exhibited better histocompatibility.

Non-degradable and degradable meshes each have their own advantages. The most considerable advantage of non-degradable meshes is the low rate of recurrence; the hernia recurrence rate after repair with PP meshes was only 4 % [45]. However, a randomized controlled trial showed that non-absorbable meshes demonstrated superior 2-year hernia recurrence risk compared with biologic mesh in patients undergoing single-stage repair of contaminated ventral hernias [26]. Therefore, whether non-absorbable mesh can truly reduce the recurrence rate of hernia still needs to be explored. Although coatings are applied to PP meshes, it is still difficult to change the fact that PP meshes cause abdominal adhesions. Some rats developed mild adhesions on the 14th and 90th days after SF-PP mesh implantation [16]. Some complications, such as poor healing of abdominal incisions, were experienced with the PLA-SRL-PP mesh. As the concentration of SRL increases, mild inflammation, foreign body reaction, mild collagen deposition, and neovascularization occur [15]. In our study, we designed a biologic mesh, which avoids the complications of non-absorbable meshes while ensuring the physical properties. The advantage of degradable meshes is that they can reduce chronic postoperative pain, foreign body sensation and delayed mesh infection. Furthermore, the degradation rates of the PLA-SF mesh were slower than the tissue repair rates, avoiding the recurrence of hernia.

Myofibroblasts play a crucial role in secreting molecules, including collagens, proteoglycans/glycosaminoglycans, elastin, fibronectin, laminins, and several other glycoproteins, which are vital components of the extracellular matrix (ECM) [46]. Excessive deposition of ECM can cause fibrosis [47]. Adhesions are fibrotic scars that form between abdominal organs following surgery or infection [48].

Adhesions arise from disordered wound healing. Using peritoneal repair caused by surgical trauma as an example, completing the repair within the first three days typically prevents the occurrence of adhesions. However, if repair and/or fibrinolysis are delayed, fibroblast proliferation can lead to the formation of adhesions [49]. Hence, in normal conditions, tissue repair follows an orderly process, while the formation of adhesions is counterproductive to effective wound healing.

Normally, When the body is subjected to harmful stimuli (such as inflammation and mechanical stress caused by the mesh), myofibroblasts derived from multiple sources (including resident fibroblasts, mesenchymal cells, circulating fibroblasts) can initiate wound healing responses by remodeling the extracellular environment [50–52]. When the tissue repair is complete, this profibrotic program shuts down. However, chronic inflammation can lead to dysregulation of this process, leading to deposition of ECM. The interplay of inflammation and mechanical stimulation can disrupt the orderly process of repair, giving rise to disordered adhesions.

The degradability of materials is also intricately linked to the formation of adhesions. The PLA-SF mesh avoided long-term contact of foreign bodies with the body, reduced inflammation and mechanical stress, thereby reducing excessive accumulation of ECM, and the TGF-β/Samd pathway was not overactivated. The non-degradable PP mesh caused the body to be in an environment of sterile inflammation and mechanical stress for a long time, and the ECM continued to deposit, which led to a large release of TGF-β1 (a major effector of the fibrotic process) [53]. Furthermore, Smad 2/3 phosphorylated by TGF-β1 bind to Smad4 and enters the nucleus, which enhances fibroblast-myofibroblast differentiation and the production and secretion of ECM [54].

The hydrophilicity of PLA-SF additionally diminishes the formation of adhesions between it and abdominal organs. Bacakova et al. suggested that highly hydrophilic surfaces prevent the adsorption of proteins, or these molecules are bound very weakly. In contrast, on highly hydrophobic materials, proteins are adsorbed in rigid and denatured forms, impeding cell adhesion [55]. This could be attributed to the fact that hydrophilic materials promote cell-matrix adhesion, whereas hydrophobic materials facilitate protein-matrix adhesion. In this study, the PLA-SF mesh exhibited higher hydrophilic, and the results of immunofluorescence (the expression of α-SMA decrease) and Masson staining (the expression of Collagen decrease) suggested that the ECM deposition caused by PLA-SF mesh was less compared to that caused by PLA mesh. This happened to attenuate the effect of the TGF-β/Samd adhesion-promoting pathway, making the repair effect milder.

The small pore structure of the PLA-SF mesh facilitated tissue repair. The results of tissue immunofluorescence (the expression of PDPN and CD31 increase) suggested that a significant influx of peritoneal mesothelial cells and new blood vessels into the PLA-SF mesh. However, the PP mesh has large pores, it was difficult for peritoneal mesothelial cells to cling, and new blood vessels only existed around the pore.

The hydrophilicity of the PLA-SF mesh might promote tissue repair. Etesabi et al. demonstrated enhanced cell proliferation and attachment to modified hydrophilic scaffold [56], a phenomenon potentially linked to the hydrophilicity of PLA-SF.

Increased production of extracellular matrix (ECM) components: Collagen I and collagen III, hyaluronan (HA), fibronectin (FN), and extra domain A fibronectin (EDA–FN) distinguish the hallmarks of myofibroblasts [57]. Collagen I and collagen III play an important role in wound healing. Henriksen et al. [38] found that a high collagen I/collagen III ratio was more conducive to hernia formation and recurrence. In this study, Western blot showed that the expression of collagen I was the highest and the expression of collagen III was the lowest in the PLA-SF group, so the ratio of collagen I/collagen III was the highest in the PLA-SF group. Therefore, the rates of tissue remodeling in the PLA-SF mesh group were the fastest, which was more conducive to tissue remodeling.

The PLA-SF mesh may be fabricated for mechanical enhancements and chemical modifications to achieve specific functionalities. Mechanical properties may improve through weaving methods, preparation processes, and the incorporation of reinforcing materials. Chemical modifications or filling with functional materials, offer versatile ways to enhance surface functionality. Zhou and his team used adipose stem cells to fill poly(ε-caprolactone)/chitosan scaffolds to promote tissue

remodeling [58]. Another study demonstrated the efficacy of a specific drug carrier system for postoperative analgesia [59]. These instances prompt speculation that PLA-SF mesh, upon chemical modification, could potentially exhibit antibacterial, anti-inflammatory, analgesic properties, and contribute to tissue remodeling. PLA-SF scaffold, following chemical modification, can be tailored for applications such as biomedical implants, drug delivery, or tissue engineering scaffolds. Yan et al. demonstrated hydrogel carriers for sustained release on stem cells, indicating potential combinations with PLA-SF scaffolds [60]. Overall, PLA-SF mesh can undergo upgrades and modifications, serving as a platform for creating materials with enhanced functionalities.

In this study, for the first time, we used behavioral experiments to evaluate the postoperative pain in a rat abdominal wall hernia model and used the rat movement distance to evaluate the effect of different meshes on postoperative pain. Furthermore, we performed small-animal CT on rats, and we could easily observe the postoperative adhesions without sacrificing the animals. Most importantly, the PLA-SF mesh not only overcame the poor mechanical properties of PLA but also reduced postoperative complications caused by PLA or PP.

5. Conclusion

The PLA-SF mesh had advantageous physicochemical properties, promoted cell proliferation and tissue remodeling through the TGF-β1/Smad pathway, reduced the expression of fibrotic molecules without producing more inflammatory factors, and led to little production of adhesions. Therefore, the PLA-SF mesh is a promising composite biological material for hernia repair.

Availability of data and materials

Data supporting the findings of this study are available from the corresponding author upon request.

CRediT authorship contribution statement

Xingjie Wang: Writing - original draft, Methodology, Formal analysis, Investigation. **Changjun Liu:** Writing - review & editing, Resources, Funding acquisition, Methodology. **Xuqi Li:** Conceptualization, Project administration, Writing - review & editing, Funding acquisition. **Tianli Shen:** Formal analysis. **Jie Lian:** Formal analysis. **Jing Shi:** Visualization. **Zhengdong Jiang:** Visualization. **Guanglin Qiu:** Validation, Investigation. **Yuanbo Wang:** Resources. **Er Meng:** Supervision, Funding acquisition. **Guangbing Wei:** Supervision, Funding acquisition.

Declaration of competing interest

The authors declare that they have no known competing financial interests or personal relationships that could have appeared to influence the work reported in this paper.

Data availability

Data will be made available on request.

Acknowledgement

This work was supported by the National Nature Science Foundation of China (Grant No. 81970456), the Shaanxi Key Research and Development Program (No. 2022SF-228), and the Scientific Research Starting Foundation for Ph.D. of Hunan University of Science and Technology (No. E51992 and No. E51993). The Graphical abstract was created with BioRender.com.

Appendix A. Supplementary data

Supplementary data to this article can be found online at https://doi.org/10.1016/j.mtbio.2023.100915.

References

[1] M.G. Franz, The biology of hernias and the abdominal wall, Hernia : the Journal of Hernias and Abdominal Wall Surgery 10 (2006) 462–471, https://doi.org/10.1007/s10029-006-0144-9.
[2] Y. Xiaolong, H. Xiaoyan, W. Bo, H. Jianglong, Y. Xiaofeng, T. Xiao, Z. Zongheng, L. Linbo, Z. Zefeng, W. Hongbo, Ventral hernia repair in rat using nanofibrous polylactic acid/polypropylene meshes, Nanomedicine 13 (2018) 2187–2199, https://doi.org/10.2217/nnm-2018-0165.
[3] U.A. Dietz, S. Menzel, J. Lock, A. Wiegering, The treatment of incisional hernia, Dtsch Arztebl Int 115 (2018) 31–37, https://doi.org/10.3238/arztebl.2018.0031.
[4] D.P.V. Lambrichts, G.H.J. de Smet, R.D. van der Bogt, L.F. Kroese, A.G. Menon, J. Jeekel, G.J. Kleinrensink, J.F. Lange, Incidence, risk factors and prevention of stoma site incisional hernias: a systematic review and meta-analysis, Colorectal Disease, the Official Journal of the Association of Coloproctology of Great Britain and Ireland 20 (2018) O288–O303, https://doi.org/10.1111/codi.14369.
[5] Y. Bilsel, I. Abci, The search for ideal hernia repair; mesh materials and types, Int. J. Surg. 10 (2012) 317–321, https://doi.org/10.1016/j.ijsu.2012.05.002.
[6] C. Clancy, P. Jordan, P.F. Ridgway, Polypropylene mesh and systemic side effects in inguinal hernia repair: current evidence, Ir, J. Med. Sci. 188 (2019) 1349–1356, https://doi.org/10.1007/s11845-019-02008-5.
[7] T. Ünek, S. Sökmen, T. Egeli, V. Avkan Oğuz, H. Ellidokuz, F. Obuz, The results of expanded-polytetrafluoroethylene mesh repair in difficult abdominal wall defects, Asian J. Surg. 42 (2019) 131–143, https://doi.org/10.1016/j.asjsur.2017.12.001.
[8] S. Todros, P.G. Pavan, A.N. Natali, Synthetic surgical meshes used in abdominal wall surgery: Part I-materials and structural conformation, J. Biomed. Mater. Res. B Appl. Biomater. 105 (2017) 689–699, https://doi.org/10.1002/jbm.b.33586.
[9] S. Yu, W. Shi, S. Houshyar, X. Wang, P. Ma, Preparation and performances of coated polypropylene hernia mesh with natural biomaterials, Colloid and Interface Science Communications 45 (2021), 100535, https://doi.org/10.1016/j.colcom.2021.100535.
[10] F. Heymann, K.-T. von Trotha, C. Preisinger, P. Lynen-Jansen, A.A. Roeth, M. Geiger, L.J. Geisler, A.K. Frank, J. Conze, T. Luedde, C. Trautwein, M. Binnebösel, U.P. Neumann, F. Tacke, Polypropylene mesh implantation for hernia repair causes myeloid cell-driven persistent inflammation, JCI Insight 4 (2019), https://doi.org/10.1172/jci.insight.123862.
[11] M. Rutegård, M. Lindqvist, J. Svensson, P. Nordin, M.M. Haapamäki, Chronic pain after open inguinal hernia repair: expertise-based randomized clinical trial of heavyweight or lightweight mesh, Br. J. Surg. 108 (2021) 138–144, https://doi.org/10.1093/bjs/znaa049.
[12] W. Hu, Z. Zhang, L. Zhu, Y. Wen, T. Zhang, P. Ren, F. Wang, Z. Ji, Combination of polypropylene mesh and in situ injectable mussel-inspired hydrogel in laparoscopic hernia repair for preventing post-surgical adhesions in the piglet model, ACS Biomater. Sci. Eng. 6 (2020) 1735–1743, https://doi.org/10.1021/acsbiomaterials.9b01333.
[13] M.R. Arnold, A.M. Kao, J. Otero, J.E. Marx, V.A. Augenstein, R.F. Sing, P. D. Colavita, K. Kercher, B.T. Heniford, Mesh fistula after ventral hernia repair: what is the optimal management? Surgery 167 (2020) 590–597, https://doi.org/10.1016/j.surg.2019.09.020.
[14] K. Baylón, P. Rodríguez-Camarillo, A. Elías-Zúñiga, J.A. Díaz-Elizondo, R. Gilkerson, K. Lozano, Past, present and future of surgical meshes: a review, Membranes 7 (2017), https://doi.org/10.3390/membranes7030047.
[15] Z. Zhang, L. Zhu, W. Hu, J. Dai, P. Ren, X. Shao, B. Xiong, T. Zhang, Z. Ji, Polypropylene mesh combined with electrospun poly (L-lactic acid) membrane in situ releasing sirolimus and its anti-adhesion efficiency in rat hernia repair, Colloids Surf. B Biointerfaces 218 (2022), 112772, https://doi.org/10.1016/j.colsurfb.2022.112772.
[16] F. Luan, W. Cao, C. Cao, B. Li, X. Shi, C. Gao, Construction and properties of the silk fibroin and polypropylene composite biological mesh for abdominal incisional hernia repair, Front. Bioeng. Biotechnol. 10 (2022), 949917, https://doi.org/10.3389/fbioe.2022.949917.
[17] R. Kaufmann, L. Timmermans, Y.T. van Loon, J.P.A.M. Vroemen, J. Jeekel, J. F. Lange, Repair of complex abdominal wall hernias with a cross-linked porcine acellular matrix: cross-sectional results of a Dutch cohort study, Int. J. Surg. 65 (2019) 120–127, https://doi.org/10.1016/j.ijsu.2019.03.023.
[18] Z. Liu, X. Liu, L. Bao, J. Liu, X. Zhu, X. Mo, R. Tang, The evaluation of functional small intestinal submucosa for abdominal wall defect repair in a rat model: potent effect of sequential release of VEGF and TGF-β1 on host integration, Biomaterials 276 (2021), 120999, https://doi.org/10.1016/j.biomaterials.2021.120999.
[19] J.S. Fernandez-Moure, J.L. Van Eps, L.E. Peterson, B.A. Shirkey, Z.K. Menn, F. J. Cabrera, A. Karim, E. Tasciotti, B.K. Weiner, W.A. Ellsworth, Cross-linking of porcine acellular dermal matrices negatively affects induced neovessel formation using platelet-rich plasma in a rat model of hernia repair, Wound Repair and Regeneration, Official Publication of the Wound Healing Society [and] the European Tissue Repair Society 25 (2017), https://doi.org/10.1111/wrr.12508.
[20] W. Huang, S. Ling, C. Li, F.G. Omenetto, D.L. Kaplan, Silkworm silk-based materials and devices generated using bio-nanotechnology, Chem. Soc. Rev. 47 (2018) 6486–6504, https://doi.org/10.1039/c8cs00187a.

[21] F. Schäfer-Nolte, K. Hennecke, K. Reimers, R. Schnabel, C. Allmeling, P.M. Vogt, J. W. Kuhbier, U. Mirastschijski, Biomechanics and biocompatibility of woven spider silk meshes during remodeling in a rodent fascia replacement model, Ann. Surg. 259 (2014) 781–792, https://doi.org/10.1097/SLA.0b013e3182917677.
[22] S. Minardi, F. Taraballi, X. Wang, F.J. Cabrera, J.L. Van Eps, A.B. Robbins, M. Sandri, M.R. Moreno, B.K. Weiner, E. Tasciotti, Biomimetic collagen/elastin meshes for ventral hernia repair in a rat model, Acta Biomater. 50 (2017) 165–177, https://doi.org/10.1016/j.actbio.2016.11.032.
[23] M. Fujii, R. Tanaka, Porcine small intestinal submucosa alters the biochemical properties of wound healing: a narrative review, Biomedicines 10 (2022), https://doi.org/10.3390/biomedicines10092213.
[24] G. Cao, Y. Huang, K. Li, Y. Fan, H. Xie, X. Li, Small intestinal submucosa: superiority, limitations and solutions, and its potential to address bottlenecks in tissue repair, J. Mater. Chem. B 7 (2019) 5038–5055, https://doi.org/10.1039/c9tb00530g.
[25] B. Andrée, A. Bär, A. Haverich, A. Hilfiker, Small intestinal submucosa segments as matrix for tissue engineering: review, Tissue Eng., Part B 19 (2013) 279–291, https://doi.org/10.1089/ten.TEB.2012.0583.
[26] M.J. Rosen, D.M. Krpata, C.C. Petro, A. Carbonell, J. Warren, B.K. Poulose, A. Costanzo, C. Tu, J. Blatnik, A.S. Prabhu, Biologic vs synthetic mesh for single-stage repair of contaminated ventral hernias: a randomized clinical trial, JAMA Surg 157 (2022) 293–301, https://doi.org/10.1001/jamasurg.2021.6902.
[27] A. Florczak, T. Deptuch, K. Kucharczyk, H. Dams-Kozlowska, Systemic and local silk-based drug delivery systems for cancer therapy, Cancers 13 (2021), https://doi.org/10.3390/cancers13215389.
[28] S. Chen, M. Liu, H. Huang, L. Cheng, H.-P. Zhao, Mechanical properties of Bombyx mori silkworm silk fibre and its corresponding silk fibroin filament: a comparative study, Mater. Des. 181 (2019), 108077, https://doi.org/10.1016/j.matdes.2019.108077.
[29] H. Xie, J. Wang, Y. He, Z. Gu, J. Xu, L. Li, Q. Ye, Biocompatibility and safety evaluation of a silk fibroin-doped calcium polyphosphate scaffold copolymer in vitro and in vivo, RSC Adv. 7 (2017) 46036–46044, https://doi.org/10.1039/c7ra04999d.
[30] W. Zhang, L. Chen, J. Chen, L. Wang, X. Gui, J. Ran, G. Xu, H. Zhao, M. Zeng, J. Ji, L. Qian, J. Zhou, H. Ouyang, X. Zou, Silk fibroin biomaterial shows safe and effective wound healing in animal models and a randomized controlled clinical trial, Adv. Healthcare Mater. 6 (2017), https://doi.org/10.1002/adhm.201700121.
[31] R. Deshpande, S. Shukla, A. Kale, N. Deshmukh, A. Nisal, P. Venugopalan, Silk fibroin microparticle scaffold for use in bone void filling: safety and efficacy studies, ACS Biomater. Sci. Eng. 8 (2022) 1226–1238, https://doi.org/10.1021/acsbiomaterials.1c01103.
[32] D. da Silva, M. Kaduri, M. Poley, O. Adir, N. Krinsky, J. Shainsky-Roitman, A. Schroeder, Biocompatibility, biodegradation and excretion of polylactic acid (PLA) in medical implants and theranostic systems, Chem. Eng. J. (2018) 340, https://doi.org/10.1016/j.cej.2018.01.010. Lausanne, Switzerland : 1996.
[33] R.A. Ilyas, S.M. Sapuan, M.M. Harussani, M.Y.A.Y. Hakimi, M.Z.M. Haziq, M.S. N. Atikah, M.R.M. Asyraf, M.R. Ishak, M.R. Razman, N.M. Nurazzi, M.N. F. Norrrahim, H. Abral, M. Asrofi, Polylactic acid (PLA) biocomposite: processing, additive manufacturing and advanced applications, Polymers 13 (2021), https://doi.org/10.3390/polym13081326.
[34] M. Douglass, S. Hopkins, R. Pandey, P. Singha, M. Norman, H. Handa, S-Nitrosoglutathione-Based nitric oxide-releasing nanofibers exhibit dual antimicrobial and antithrombotic activity for biomedical applications, Macromol. Biosci. 21 (2021), e2000248, https://doi.org/10.1002/mabi.202000248.
[35] M.S. Singhvi, S.S. Zinjarde, D.V. Gokhale, Polylactic acid: synthesis and biomedical applications, J. Appl. Microbiol. 127 (2019) 1612–1626, https://doi.org/10.1111/jam.14290.
[36] C. Belbéoch, J. Lejeune, P. Vroman, F. Salaün, Silkworm and spider silk electrospinning: a review, Environ. Chem. Lett. 19 (2021) 1737–1763, https://doi.org/10.1007/s10311-020-01147-x.
[37] L.Y.C. Madruga, M.J. Kipper, Expanding the repertoire of electrospinning: new and emerging biopolymers, techniques, and applications, Adv. Healthcare Mater. 11 (2022), e2101979, https://doi.org/10.1002/adhm.202101979.
[38] N.A. Henriksen, D.H. Yadete, L.T. Sorensen, M.S. Agren, L.N. Jorgensen, Connective tissue alteration in abdominal wall hernia, Br. J. Surg. 98 (2011) 210–219, https://doi.org/10.1002/bjs.7339.
[39] T. Saha, S. Houshyar, S.R. Sarker, S. Pyreddy, C. Dekiwadia, Z. Nasa, R. Padhye, X. Wang, Nanodiamond-chitosan functionalized hernia mesh for biocompatibility and antimicrobial activity, J. Biomed. Mater. Res. 109 (2021) 2449–2461, https://doi.org/10.1002/jbm.a.37237.
[40] F. Marinaro, J.M. Silva, A.A. Barros, I.M. Aroso, J.C. Gómez-Blanco, I. Jardin, J. J. Lopez, M. Pulido, M.Á. de Pedro, R.L. Reis, F.M. Sánchez-Margallo, J.G. Casado, E. López, A fibrin coating method of polypropylene meshes enables the adhesion of menstrual blood-derived mesenchymal stromal cells: a new delivery strategy for stem cell-based therapies, Int. J. Mol. Sci. 22 (2021), https://doi.org/10.3390/ijms222413385.
[41] D.U. Lee, D.W. Kim, S.Y. Lee, D.Y. Choi, S.Y. Choi, K.-S. Moon, M.Y. Shon, M. J. Moon, Amino acid-mediated negatively charged surface improve antifouling and tribological characteristics for medical applications, Colloids Surf. B Biointerfaces 211 (2022), 112314, https://doi.org/10.1016/j.colsurfb.2021.112314.
[42] F.J. Calero Castro, Y. Yuste, S. Pereira, M.D. Garvín, M.Á. López García, F. J. Padillo, F. de la Portilla, Proof of concept, design, and manufacture via 3-D printing of a mesh with bactericidal capacity: behaviour in vitro and in vivo, J. Tissue Eng. Regen. Med. 13 (2019) 1955–1964, https://doi.org/10.1002/term.2944.
[43] W.S. Cobb, J.M. Burns, K.W. Kercher, B.D. Matthews, H. James Norton, B. Todd Heniford, Normal intraabdominal pressure in healthy adults, J. Surg. Res. 129 (2005) 231–235, https://doi.org/10.1016/j.jss.2005.06.015.
[44] W. Qiu, C. Zhong, R. Xu, T. Zou, F. Wang, Y. Fan, L. Wang, Z. Yang, Novel large-pore lightweight polypropylene mesh has better biocompatibility for rat model of hernia, J. Biomed. Mater. Res., Part A 106 (2018) 1269–1275, https://doi.org/10.1002/jbm.a.36326.
[45] D. Ulrich, S.L. Edwards, J.F. White, T. Supit, J.A.M. Ramshaw, C. Lo, A. Rosamilia, J.A. Werkmeister, C.E. Gargett, A preclinical evaluation of alternative synthetic biomaterials for fascial defect repair using a rat abdominal hernia model, PLoS One 7 (2012), e50044, https://doi.org/10.1371/journal.pone.0050044.
[46] A.D. Theocharis, S.S. Skandalis, C. Gialeli, N.K. Karamanos, Extracellular matrix structure, Adv. Drug Deliv. Rev. 97 (2016), https://doi.org/10.1016/j.addr.2015.11.001.
[47] N.C. Henderson, F. Rieder, T.A. Wynn, Fibrosis: from mechanisms to medicines, Nature 587 (2020) 555–566, https://doi.org/10.1038/s41586-020-2938-9.
[48] D.S. Foster, C.D. Marshall, G.S. Gulati, M.S. Chinta, A. Nguyen, A. Salhotra, R. E. Jones, A. Burcham, T. Lerbs, L. Cui, M.E. King, A.L. Titan, R.C. Ransom, A. Manjunath, M.S. Hu, C.P. Blackshear, S. Mascharak, A.L. Moore, J.A. Norton, C. J. Kin, A.A. Shelton, M. Januszyk, G.C. Gurtner, G. Wernig, M.T. Longaker, Elucidating the fundamental fibrotic processes driving abdominal adhesion formation, Nat. Commun. 11 (2020) 4061, https://doi.org/10.1038/s41467-020-17883-1.
[49] P.R. Koninckx, V. Gomel, A. Ussia, L. Adamyan, Role of the peritoneal cavity in the prevention of postoperative adhesions, pain, and fatigue, Fertil. Steril. 106 (2016), https://doi.org/10.1016/j.fertnstert.2016.08.012.
[50] M. Vierhout, A. Ayoub, S. Naiel, P. Yazdanshenas, S.D. Revill, A. Reihani, A. Dvorkin-Gheva, W. Shi, K. Ask, Monocyte and macrophage derived myofibroblasts: is it fate? A review of the current evidence, Wound Repair and Regeneration, Official Publication of the Wound Healing Society [and] the European Tissue Repair Society 29 (2021) 548–562, https://doi.org/10.1111/wrr.12946.
[51] P. Pakshir, N. Noskovicova, M. Lodyga, D.O. Son, R. Schuster, A. Goodwin, H. Karvonen, B. Hinz, The myofibroblast at a glance, J. Cell Sci. 133 (2020), https://doi.org/10.1242/jcs.227900.
[52] R. Schuster, J.S. Rockel, M. Kapoor, B. Hinz, The inflammatory speech of fibroblasts, Immunol. Rev. 302 (2021) 126–146, https://doi.org/10.1111/imr.12971.
[53] D. Peng, M. Fu, M. Wang, Y. Wei, X. Wei, Targeting TGF-β signal transduction for fibrosis and cancer therapy, Mol. Cancer 21 (2022) 104, https://doi.org/10.1186/s12943-022-01569-x.
[54] S.-Y. Heo, M.-S. Jeong, H.S. Lee, Y.J. Kim, S.-H. Park, W.-K. Jung, Phlorofucofuroeckol A from Ecklonia cava ameliorates TGF-β1-induced fibrotic response of human tracheal fibroblasts via the downregulation of MAPKs and SMAD 2/3 pathways inactivated TGF-β receptor, Biochem. Biophys. Res. Commun. 522 (2020) 626–632, https://doi.org/10.1016/j.bbrc.2019.11.127.
[55] L. Bacakova, E. Filova, M. Parizek, T. Ruml, V. Svorcik, Modulation of cell adhesion, proliferation and differentiation on materials designed for body implants, Biotechnol. Adv. 29 (2011) 739–767, https://doi.org/10.1016/j.biotechadv.2011.06.004.
[56] H. Ehtesabi, F. Massah, Improvement of hydrophilicity and cell attachment of polycaprolactone scaffolds using green synthesized carbon dots, Materials Today Sustainability 13 (2021), 100075, https://doi.org/10.1016/j.mtsust.2021.100075.
[57] Y. Tai, E.L. Woods, J. Dally, D. Kong, R. Steadman, R. Moseley, A.C. Midgley, Myofibroblasts: function, formation, and scope of molecular therapies for skin fibrosis, Biomolecules 11 (2021), https://doi.org/10.3390/biom11081095.
[58] Z. Zhou, H. Yan, Y. Liu, D. Xiao, W. Li, Q. Wang, Y. Zhao, K. Sun, M. Zhang, M. Lu, Adipose-derived stem-cell-implanted poly(ϵ-caprolactone)/chitosan scaffold improves bladder regeneration in a rat model, Regen. Med. 13 (2018) 331–342, https://doi.org/10.2217/rme-2017-0120.
[59] F. Chai, M. Maton, S. Degoutin, G. Vermet, N. Simon, C. Rousseaux, B. Martel, N. Blanchemain, In vivo evaluation of post-operative pain reduction on rat model after implantation of intraperitoneal PET meshes functionalised with cyclodextrins and loaded with ropivacaine, Biomaterials 192 (2019) 260–270, https://doi.org/10.1016/j.biomaterials.2018.07.032.
[60] H. Yan, L. Rong, D. Xiao, M. Zhang, S.P. Sheikh, X. Sui, M. Lu, Injectable and self-healing hydrogel as a stem cells carrier for treatment of diabetic erectile dysfunction, Mater. Sci. Eng., C 116 (2020), 111214, https://doi.org/10.1016/j.msec.2020.111214.